Numerical Solution and Discussion of Results

The iterative procedure, as described by Gorla,[3] is used for the circular pin and the boundary layer. The boundary-layer equations were solved by an implicit finite-difference method described by Cebeci and Bradshaw.[7]

The dimensionless local heat flux may be written as

$$\frac{q_w L}{K_f (T_0 - T_\infty) Re^{1/2}} = -\frac{\theta'(\xi,0)}{2\xi^{1/2}} \tag{11}$$

Figures 1 and 2 display the numerical results for the local heat transfer coefficients at various axial locations of the pin. It may be observed that higher values of the conjugate convection-conduction parameter N_c represent higher local heat-transfer coefficients. As the buoyancy force parameter Ω increases, the magnitude of the heat transfer coefficients also increases. As the dimensionless material parameters Δ increases, the heat transfer coefficients decrease due to the presence of polymeric additives. We may note that $\Delta = 0$ denotes Newtonian fluids. The local heat transfer coefficients do not decrease monotonically in the flow direction for large values of N_c and Ω. They decrease first to some minimum value and then steadily increase with ξ. This is attributed to enhanced buoyancy associated with an increase in the wall to fluid temperature difference along the streamwise direction.

The results for the pin temperature distribution are illustrated in Fig. 3. As N_c or Ω increases, we see that the pin surface becomes more nonisothermal. In all cases, the pin temperature distributions decrease monotomically from root to tip.

Concluding Remarks

In this Note, we have presented an analysis for the conjugate convection and conduction heat transfer including buoyancy force on the forced flow of a micropolar fluid over a vertical circular pin. The overall heat transfer rate decreases with increasing values of the convection-conduction parameter N_c or decreasing values of the buoyancy parameter. The surface temperature variations of the pin from the root to tip increase with increasing values of N_c and the buoyancy force parameter Ω.

References

[1]Sparrow, E. M., and Acharya, S., *Journal of Heat Transfer*, Transactions of American Society of Mechanical Engineers, Vol. 103, No. 2, 1981, pp. 218-225.

[2]Sparrow, E. M., and Chyu, M. K., *Journal of Heat Transfer*, Transactions of American Society of Mechanical Engineers, Vol. 104, No. 2, 1982, pp. 204-206.

[3]Gorla, R. S. R., *International Journal of Heat and Fluid Flow*, Vol. 9, No. 1, 1988, pp. 49-52.

[4]Lien, F. S., and Chen, C. K., *Journal of Heat Transfer*, Transactions of American Society of Mechanical Engineers, Vol. 108, No. 4, 1981, pp. 580-586.

[5]Gorla, R. S. R., *International Journal of Engineering Science*, Vol. 27, 1989, pp. 77-86.

[6]Moutsoglou, A., *Journal of Heat Transfer*, Transactions of American Society of Mechanical Engineers, Vol. 105, No. 4, 1983, pp. 830-836.

[7]Cebeci, T., and Bradshaw, P., *Momentum Transfer in Boundary Layers*, Hemisphere, Washington, DC, 1977.

Mixed Convection of Low Prandtl Number Fluid in the Annuli of Rotating Cylinders

T. S. Lee*
National University of Singapore, Singapore 0511

Nomenclature

$\hat{g}$	= gravitational vector
K_{eq}	= overall equivalent thermal conductivity
K_{eql}	= local equivalent thermal conductivity
L	= characteristics length, $(R_o - R_i)$
Pr	= Prandtl number, ν/α
R_i, R_o	= inner and outer cylinder radii
Ra	= Rayleigh number, $\beta g L^3 T_m/\alpha\nu$
Re	= Reynolds number, $R_i \omega L/\nu$
r	= radial coordinate
T_i, T_o	= temperatures of inner and outer cylinders
T_R, T_m	= reference temperature; $T_R = (T_i + T_o)/2$, $T_m = (T_i - T_o)/2$, respectively
t, T	= time and temperature, respectively
u, v	= radial and tangential velocity, respectively
α, β	= thermal diffusivity and coefficient of volumetric expansion
γ	= angle measured anticlockwise from the downward vertical through the center of the heater cylinder
Θ	= dimensionless temperature, $(T - T_R)/T_m$
ν	= kinematic viscosity
ρ	= reference density corresponding to T_R
ϕ	= angular coordinate
ψ, ζ	= stream function and vorticity, respectively
ω	= angular velocity of inner rotating cylinder

Introduction

CONVECTIVE fluid motion in a region bounded by two horizontal cylinders with parallel axes has been the subject of many studies in recent years. The mixed-convection problem in which buoyancy and centrifugal effects (created by heated rotating cylinders) is of practical concern in many technological applications, ranging from the control of chemical engineering process equipment, rotating machinery, and shafting, to the prediction of meteorological conditions. In machinery with the rotating shaft heated by electrical means through a mercury slip ring, the rotating shaft is immersed in mercury and the characteristics of the fluid flow and heat transfer processes are not well known. In most of the studies cited,[1-7] attention has been focused on fluids with Prandtl numbers of order one and larger, and none consider the rotating shaft immersed in mercury with a Prandtl number of 0.02. Liu et al.[1] measured overall heat transfer characteristics and temperature profiles for air, water, and silicone oil. Photographic studies of the flow patterns in air were first presented by Bishop and Carley.[2] Powe et al.[3] examined the critical Rayleigh number at which counter-rotating eddies begin to form for air. Kuehn and Goldstein[4] presented results of experimental and numerical studies of the motion of air and water within a horizontal annulus. More recent related studies were done by Fusegi et al.,[5] Bishop and Brandon,[6] and Bishop.[7] These studies, however, were concerned with fluids of $Pr \cong 1$ or higher.

Received Dec. 7, 1989; revision received April 25, 1990; accepted for publication April 26, 1990.

*Senior Lecturer, Department of Mechanical Engineering.

This Note investigates the fluid motion and heat-transfer characteristics of a fluid with a Prandtl number of 0.02 contained within a horizontal cylindrical annulus of radius ratio 2.6, following earlier experimental work by Lee et al.[8] and Kuehn and Goldstein.[4] The inner cylinder is assumed heated and rotating. The flow is assumed to be steady, two-dimensional, and laminar for the range of parameters considered here. This assumption of two-dimensional flow pattern and heat transfer was verified experimentally by Lee et al.[8] for the parameters considered with air. However, Fusegi et al.[5] proposed numerically that the limit may be lower and is decided by a rotational parameter being less than one. The effect of Prandtl-number variations was not investigated in the preceding studies.

Governing and Boundary Equations

The dimensionless governing equations that describe the motion of the incompressible fluid within the annulus in Fig. 1, subject to the Boussinesq approximation, are

$$\frac{\partial \zeta^*}{\partial t} - \nabla \times (u^* \times \zeta^*) = -RaPr \nabla \times (\Theta \hat{g}) + Pr \nabla^2 \zeta^* \quad (1)$$

$$\frac{\partial \Theta}{\partial t} + u^* \cdot \nabla \Theta = \nabla^2 \Theta \quad (2)$$

$$\zeta^* = -\nabla^2 \psi^* \quad (3)$$

$$u^* = \nabla \times \psi^* \quad (4)$$

where $r^* = r/L$, $t^* = t/(L^2/\alpha)$, $u^* = u/(\alpha/L)$, $\zeta^* = \zeta/(\alpha/L^2)$, and $\psi^* = \psi/\alpha$. (From here on the * denoting dimensionless quantity is dropped for simplicity.)

The boundary ψ is constant as there is no flow across the boundaries,

$$\psi_o = 0, \qquad \psi_i = f(Re) \quad (5)$$

where $f(Re)$ is determined by the requirement that the pressure distribution be single-valued. With the inner cylinder rotating at ω and assuming no slip at the boundaries,

$$u_i = u_o = v_o = 0, \qquad v_i = RePr \quad (6)$$

Boundary Θ and ζ are given by

$$\Theta_i = 1, \qquad \Theta_o = -1 \quad (7)$$

$$\zeta_w = -\frac{\partial^2 \psi}{\partial r^2} + \frac{v}{r} \quad (8)$$

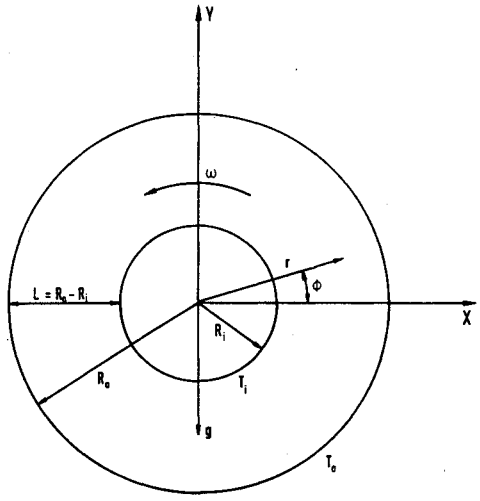

Fig. 1 Coordinate system in the annular region.

The heat transfer characteristics of the convective fluid flow pattern, when the inner cylinder is rotated, can best be described by the equivalent thermal coductivities as used by Kuehn and Goldstein[4]:

$$K_{eql} = \frac{\text{(heat transferred per unit area)}}{k(\Delta T)/[r \ell n(R_o/R_i)]} \quad (9)$$

$$K_{eq} = \frac{\text{(heat transferred per unit length)}}{2\pi k(\Delta T)/\ell n(R_o/R_i)} \quad (10)$$

For K_{eql} in Eq. (9), the radial distance r is either R_o or R_i depending on the surface considered.

Numerical Method

The finite difference solutions of Eqs. (1–4), with their boundary conditions, Eqs. (5–10), are obtained at the nodal points of a 20×60 uniform mesh superimposed on the solution region of Fig. 1. Detailed numerical procedures are described by Lee[9] and Lee et al.,[8] and will not be repeated here. The numerical solution procedures converged readily for low Prandtl numbers to the order of 0.001. Smaller Prandtl numbers were not investigated as there is no real fluid of practical interest. The solution process, however, encountered some numerical instabilities when the Prandtl number exceeded 100. The limiting cases of $Re = 0$ (i.e., stationary cylinders) or low Rayleigh number of 1000 were presented in an earlier work by Lee.[10] For $Ra = 0$ (i.e., $T_o = T_i$), investigations were carried out for verification purposes only[10] with varying Reynolds number up to a value of 1000. However, it must be pointed out that for $Re = 0$, a slightly different mathematical formulation of the problem is necessary to avoid a point of singularity in the governing equations.

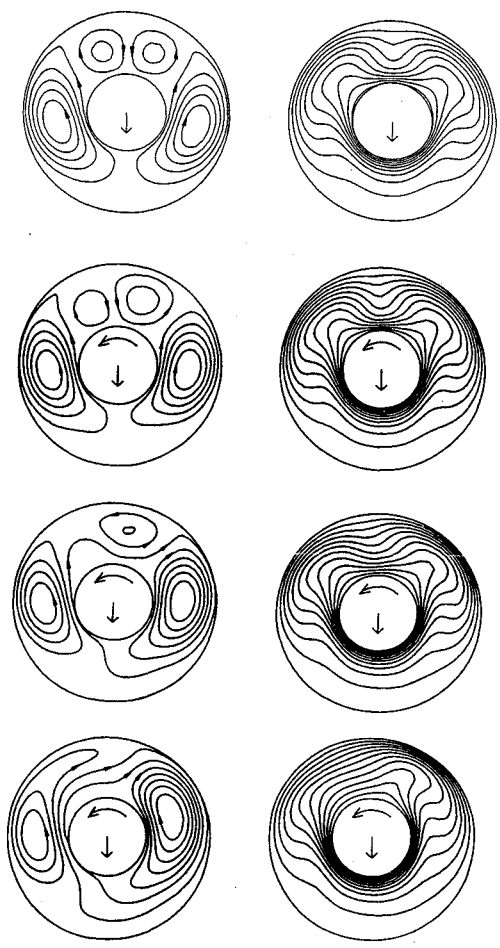

Fig. 2 Streamlines and isotherms ($R_o/R_i = 2.6$, $Ra = 5.5 \times 10^4$, $Pr = 0.02$): a) $Re = 0$; b) $Re = 140$; c) $Re = 416$; and d) $Re = 1120$.

Results and Conclusions

For fluids with low Prandtl number, the present investigation (Fig. 2a) shows a multicellular flow pattern that contrasts with the usual monocellular flowfield obtained for high Prandtl number fluids.[4,11] As a consequence of this multicellular flow pattern, the heat transfer characteristics for fluids with low Prandtl number were found to have points of maximum and minimum at the interior nodes, instead of the top and bottom nodes which is known for the high Prandtl number fluids. When the inner cylinder is made to rotate, the multicellular flow pattern on one side of the annulus is suppressed. There is an imbalance in the magnitudes of the buoyancy and shear forces such that the thermal plume moves in the direction opposite to that of the inner rotating cylinder. This thermal plume movement is distinctly different and opposite to that observed for the high Prandtl number fluid flow, where the monothermal plume on top of the inner cylinder moves in the same direction as the inner rotating cylinder.[8]

The development of the counter-rotating secondary cells and bithermal plumes for a fluid with a Prandtl number of 0.02, at a Rayleigh number of 5.5×10^4, is shown in Fig. 2. At a low Reynolds number of 140 (Fig. 2b), two counter-rotating secondary cells of different strengths are formed above the inner cylinder. Because of the occurrence of these counter-rotating secondary cells, a pair of thermal plumes are observed above the inner cylinder at an approximate angle of 45 deg on both sides of the vertical axis. With the rotation of the inner cylinder in the counterclockwise direction, it is noted that the left counter-rotating secondary cell is smaller than the right

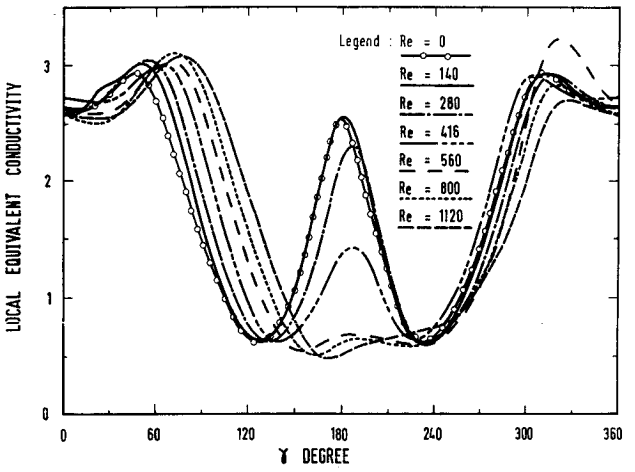

Fig. 3 Local equivalent thermal conductivity of inner cylinder ($R_o/R_i = 2.6$, $Ra = 5.5 \times 10^4$, $Pr = 0.02$).

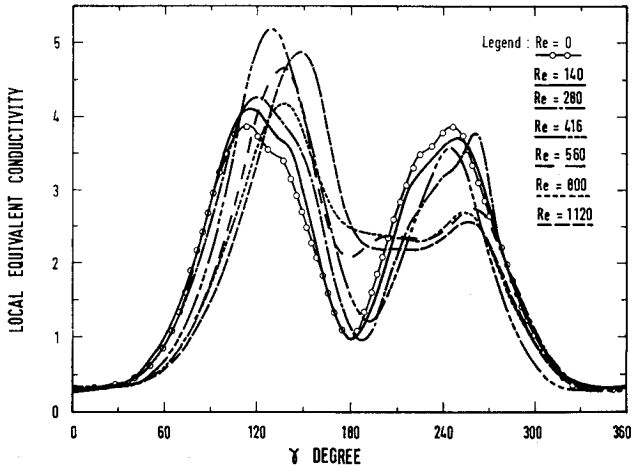

Fig. 4 Local equivalent thermal conductivity of outer stationary cylinder ($R_o/R_i = 2.6$, $Ra = 5.5 \times 10^4$, $Pr = 0.02$).

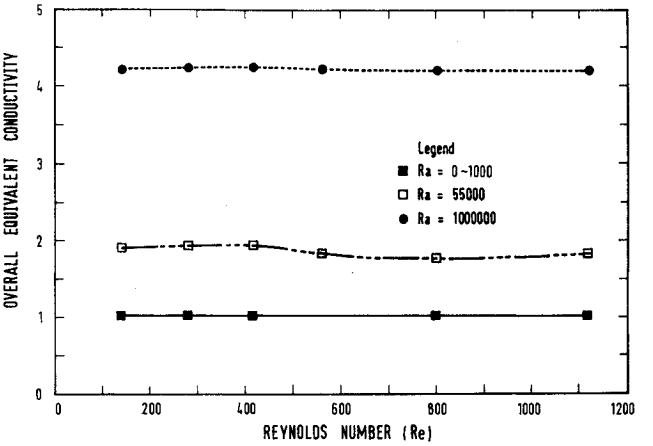

Fig. 5 Overall equivalent thermal conductivity at various Rayleigh numbers ($R_o/R_i = 2.6$, $Pr = 0.02$).

counter-rotating secondary cell. As the Reynolds number is increased, the size of the left counter-rotating secondary cell decreases further. The zero-value streamline eventually enveloped the right counter-rotating secondary cell. At the same time, it is noted that the bithermal plume on the left side of the inner cylinder is gradually suppressed. Increasing the angular speed to the Reynolds number of 416 (Fig. 2c), it is seen that the left-hand secondary cell diminishes and there is now only a single counter-rotating cell formed above the inner rotating cylinder. The thermal plume on the left-hand side continued to be suppressed further. As the Reynolds number further increases, the remaining counter-rotating secondary cell also gradually decreases its size and is eventually enveloped by the left-hand main cell. A marked decrease in the left-hand thermal plume can be observed. In the Reynolds number range of 800–1120 (Fig. 2d), the remaining counter-rotating secondary cell disappeared and the left-hand thermal plume "leveled off," giving the observed the impression that the thermal plume had moved in the opposite direction to that of the inner cylinder rotational direction.

As shown in Figs. 3 and 4, at a Rayleigh number of 5.5×10^4, the distribution of the local equivalent thermal conductivity at the inner and outer cylinders is greatly influenced by the development and modification of the multicellular flow pattern due to the rotation of the inner cylinder. Arising from the suppression of the left thermal plume, the peak heat flux on the outer cylinder takes on two different values: the peak value for the right-hand thermal plume being higher than that of the left-hand thermal plume. As the Reynolds number is increased, the peak local heat flux near the left-hand thermal plume gradually leveled off. For the inner cylinder, the local peak value near the top of the cylinder gradually leveled off as the Reynolds number is increased.

For the case of the low Prandtl number of 0.02, Fig. 5 shows that as the Rayleigh number increases the overall equivalent thermal conductivity increases. This is expected as the mode of heat transfer changes from conduction to convection as the Rayleigh number increases. However, for a particular Rayleigh number, the variation of the overall equivalent thermal conductivity is negligible when the Reynolds number is increased. In the Rayleigh number range of 0–1000, there is not much variation in the overall equivalent thermal conductivity value. For the case of a Rayleigh number of 10^3, the overall equivalent thermal conductivity varies from a minimum of 1.02 at a Reynolds number of 140 to a maximum of 1.10 at a Reynolds number of 1120. The value of the overall thermal conductivity is approximately 1.0, indicating that the mode of heat transfer is essentially conduction. When the Rayleigh number is increased to 5.5×10^4, it was noted that the overall thermal conductivity varies between a maximum value of 1.94 and a minimum value of 1.77. A similar trend for the overall thermal conductivity was also observed for the case of a Ray-

leigh number of 10^6. The overall thermal conductivity value varies between a maximum of 4.23 at a Reynolds number of 416 and a minimum value of 4.19 at a Reynolds number of 1120. From the preceding studies, it can be concluded that for a given Rayleigh number in the range of 10^3–10^6, the overall equivalent thermal conductivity is almost constant with respect to the rotational Reynolds number in the range of 0–10^3, although the streamlines, isotherms, and local equivalent thermal conductivity exhibits very different features.

References

[1]Liu, C. Y., Mueller, W. K., and Landis, F., "Natural Convective Heat Transfer in Long Horizontal Cylindrical Annuli," *International Developments in Heat Transfer, ASME*, Pt. 4, 1961, pp. 976–984.

[2]Bishop, E. H., and Carley, C. T., "Photographic Studies of Natural Convection Between Concentric Cylinders," *Proceedings of the 1966 Heat Transfer Fluid Mechanics Institute*, Stanford Univ. Press, Stanford, CA, 1966, pp. 63–78.

[3]Powe, R. E., Carley, C. T., and Carruth, S. L., "A Numerical Solution for Natural Convection in Cylindrical Annuli," *ASME Journal of Heat Transfer*, Vol. 93, No. 12, 1971, pp. 210–220.

[4]Kuehn, T. H., and Goldstein, R. J., "An Experimental and Theoretical Study of Natural Convection in the Annulus Between Horizontal Concentric Cylinders," *Journal of Fluid Mechanics*, Vol. 74, No. 4, 1976, pp. 695–719.

[5]Fusegi, T., Farouk, B., and Ball, K. S., "Mixed-Convection Flows Within a Horizontal Concentric Annulus with a Heated Rotating Inner Cylinder," *Numerical Heat Transfer*, Vol. 9, No. 2, 1986, pp. 591–604.

[6]Bishop, E. H., and Brandon, S. C., "Heat Transfer by Natural Convection of Gases Between Horizontal Isothermal Concentric Cylinders: The Expansion Number Effect," *Proceedings ASME/JSME Thermal Engineering Joint Conference*, Vol. 2, American Society of Mechanical Engineers, New York, 1987, pp. 275–280.

[7]Bishop, E. H., "Heat Transfer by Natural Convection of Helium Between Horizontal Isothermal Concentric Cylinders at Cryogenic Temperatures," *Journal of Heat Transfer*, Vol. 110, No. 1, 1988, pp. 109–115.

[8]Lee, T. S., Wijeysundera, N. E., and Yeo, K. S., "Convection in Eccentric Annuli with Inner Cylinder Rotation," *AIAA Journal*, Vol. 24, No. 1, 1986, pp. 170–171.

[9]Lee, T. S., "Numerical Experiments with Laminar Fluid Convection Between Concentric and Eccentric Heated Rotating Cylinders," *International Journal of Numerical Heat Transfer*, Vol. 7, No. 1, 1984, pp. 77–87.

[10]Lee, T. S., "Free and Forced Convection in Concentric and Eccentric Horizontal Cylindrical Annuli," *Proceedings of the ASME/JSME Thermal Engineering Joint Conference*, Vol. 3, American Society of Mechanical Engineers, New York, 1983, pp. 125–131.

[11]Lee, T. S., Wijeysundera, N. E., and Yeo, K. S., "Convective Fluid Motion and Heat Transfer in Concentric and Eccentric Cylindrical Collector System," ASME Solar Energy Division, *Proceedings of Sixth Annual Technical Conference*, Las Vegas, NV, 1984, pp. 194–200.

Two-Dimensional Effects in a Triangular Convecting Fin

A. Aziz* and H. Nguyen†

Gonzaga University, Spokane, Washington 99258

Introduction

THE traditional approach to the analysis and design of fins is based on the assumption of one-dimensional conduction in the fin material. In recent years, however, several workers have studied the effect of two-dimensional conduction on the performance of fins. For example, Lau and Tan[1] used the method of separation of variables to develop exact solutions for two-dimensional conduction in straight and annular fins of rectangular profile. A similar approach for a cylindrical fin was used by Irey.[2] These exact solutions show that the one-dimensional assumption is valid only if the Biot number (Bi) based on half thickness of the fin is much less then one, otherwise the errors can be as high as 60% for $Bi = 10$. The validity criterion of $Bi \ll 1$ was established analytically by Levitsky[3] who showed that the exact solution for three-dimensional conduction in an infinitely long rectangular fin does indeed reduce to the standard one-dimensional solution if $Bi \ll 1$.

Since the two-dimensional triangular fin does not admit an exact analytical solution, the problem has been studied by Sfeir[4] and Burmeister[5] using an approximate technique. Both authors used a heat balance integral approach to reduce the two-dimensional heat conduction equation to an ordinary differential equation. While Sfeir solved the equation numerically, Burmeister obtained the solution in terms of hypergeometric functions. Since numerical solutions of the problem are not available, it is not possible to assess the accuracy of these approximate results. In any case, the results presented in these two papers do not provide a quantitative picture of how the Biot number and length-to-base thickness ratio affect the heat transfer rate and the magnitude of the errors introduced due to the one-dimensional assumption.

The purpose of this work is twofold. The first purpose is to obtain a finite element solution for the two-dimensional triangular fin and present the heat transfer data for a wide range of Biot number and length-to-base thickness ratio so that the information can be used for prediction as well as design purposes. The second purpose is to report additional data for the rectangular fin to supplement the results of Lau and Tan.[1]

Analysis

Consider a triangular fin of length L and base thickness w attached to a primary surface at temperature T_b (shown as inset in Fig. 2). The fin is convecting heat from both its sloping faces to an environment at temperature T_∞, the heat transfer coefficient being h. Because of thermal symmetry, we analyze one-half of the fin. For two-dimensional conduction, the governing equation and boundary conditions in dimensionless form are

$$\frac{\partial^2\theta}{\partial X^2} + \frac{\partial^2\theta}{\partial Y^2} = 0 \tag{1}$$

$$\theta(0,Y) = 1, \qquad \frac{\partial\theta}{\partial Y}(X, 0) = 0, \qquad \nabla\theta \cdot \vec{n} = -Bi\,\theta \text{ on sloping surface} \tag{2}$$

where $\theta = (T - T_\infty)/(T_b - T_\infty)$, $X = \alpha x/L$, $Y = y/(w/2)$, $Bi = hw/2k$, $\alpha = L/(w/2)$, and $\vec{n}$ is the outward normal vector. In Eq. (2), the first condition represents the constant base (root) temperature. The second condition is the result of thermal symmetry (symmetrical temperature distribution about $y = 0$). The last condition corresponds to convective dissipation from the sloping surface to the environment.

The total heat transfer, q_2 (subscript 2 denotes the two-dimensional solution) per unit depth of the fin can be expressed in dimensionless form as

$$Q_2 = \frac{q_2}{k(T_b - T_\infty)} = -\frac{2}{\alpha}\int_0^1 \left.\frac{\partial\theta}{\partial X}\right|_{X=0} dY \tag{3}$$

Equations (1) and (2) were solved using a finite element approach. The solution was subsequently used to evaluate Q_2

Received April 9, 1990; revision received Sept. 19, 1990; accepted for publication Sept. 30, 1990.

*Professor, Department of Mechanical Engineering.

†Visiting Assistant Professor, Department of Mechanical Engineering.